ACS APPLIED MATERIALS & INTERFACES

Research Article

www.acsami.org

Intracellular pH-Triggered, Targeted Drug Delivery to Cancer Cells by Multifunctional Envelope-Type Mesoporous Silica Nanocontainers

Ke Yang,*[,†,‡] Huaiqing Luo,[†] Ming Zeng,[†] Yinyan Jiang,[†] Jianming Li,*[,†] and Xinling Fu[†]

[†]Department of Human Anatomy, Histology and Embryology, College of Basic Medical Sciences, Changsha Medical University, Changsha, 410219, China

[‡]College of Biology, Hunan University, Changsha 410082, China

Supporting Information

ABSTRACT: In this work, a novel type of pH-sensitive multifunctional envelope-type mesoporous silica nanocontainers (SBDAPF) was constructed for targeted drug delivery to cancer cells. Poly(*N*-succinimidyl acrylate) was coated on the mesoporous silica nanoparticles surface via an acid-labile acetal linker to obtain the SBA particles for pH-triggered drug release. A model drug doxorubicin (DOX)-loaded SBA system (SBDA) showed low premature drug release at neutral pH and effective stimuli-responsive release under the acidic conditions. To provide the colloidal stability and avoid nonspecific uptake of normal or healthy cells, the SBDA nanocontainers were modified with a poly(ethylene glycol) (PEG) polymer to form a protection layer. Furthermore, folic acid was introduced as a targeting component and anchored on the PEG outer layer to achieve the cancer-targeting ability. In vitro study demonstrated that SBDAPF could selectively adhere to the surface of cancer cells through the specific binding with folate receptor and be internalized into cells, subsequently releasing the entrapped DOX with high efficiency in slightly acidic intracellular microenvironment to finally kill cancer cells. Such a versatile drug delivery system as SBDAPF should have a potential application in cancer therapy.

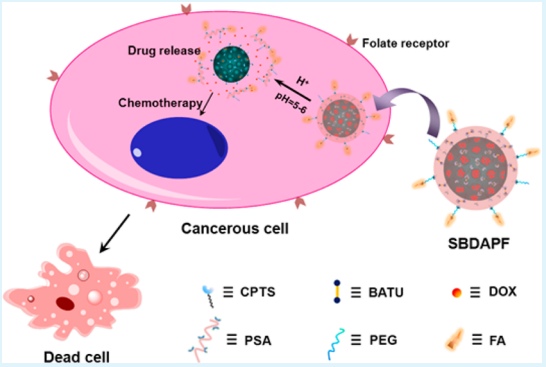

KEYWORDS: *envelope-type silica nanocontainers, targeted drug delivery, pH-response, controlled drug release, folic acid*

INTRODUCTION

For cancer therapy, drug delivery systems (DDSs) have gained much importance in optimizing the anticancer efficacy of antineoplastic drugs.[1] To enhance the therapeutic index and reduce the toxic side effects of drugs during chemotherapy, massive research efforts have been dedicated to developing smart stimuli-responsive DDSs, which release effective dosage drug at the right time.[2] In the past decades, mesoporous silica nanoparticles (MSNs) have attracted great attention as a potential drug container because of their facile synthesis, tunable pore diameter, easy surface-functionalization, low toxicity, and large capacity to carry disparate payloads within the mesoporous channels.[3−6] Several smart DDSs based on MSNs were reported for regulating the release of drugs by diverse stimuli including light,[7,8] temperature,[9] redox,[10,11] pH,[12,13] enzymes,[14] etc. Among these stimuli, pH-induced activation is a readily and convenient method by a simple addition of base or acid. More importantly, the oxygen overconsumption at inflammatory site or tumor tissue can lead to the generation of an acidic microenvironment. In addition, both endosomes and lysosomes in living cells formed after uptake of DDSs are also slightly acidic.[12,15] Consequently, a variety of pH-responsive DDSs have been developed to deliver drugs triggered by a pH signal, especially an acidic pH. Up to now, there are mainly five kinds of acid-sensitive mechanisms involving decrease of electrostatic interaction,[16,17] hydrophilic to hydrophobic transition,[15,18] conformational variation of capping agents,[19] dissolution of pore blockage,[12,20,21] and cleavage of acid-labile bonds.[13,22,23] In spite of these extensive developments, the previously reported acid-responsive DDSs have still some disadvantages; for instances, poor water dispersibility, unspecific uptake by normal cells and the cytotoxicity of the pore-blocking agents used.

Biocompatible polymers as pore-blocking agents display many distinctive properties, such as providing the colloidal stability, improving water dispersibility and biocompatibility of DDSs, facilitating conjugation of targeting components, and reducing unspecific cell uptake,[24,25] which were crucial for efficient chemotherapy. Therefore, coating a biocompatible polymer on MSNs surface to seal the pore mouths is a promising approach for construction of the desired acid-responsive DDSs. In these reported systems, polymers were coated on the surface of MSNs mainly by noncovalent interaction and in situ polymerization.[26,27] However, both of these strategies have some limitations. Noncovalent assembly is prone to premature drug release and aggregation and rapid

Received: May 28, 2015
Accepted: July 21, 2015
Published: July 21, 2015

DOI: 10.1021/acsami.5b04684
ACS Appl. Mater. Interfaces 2015, 7, 17399−17407

Scheme 1. Construction of SBDAPF as a Multifunctional pH-Sensitive Envelope-Type Mesoporous Silica Nanocontainers for Targeted Drug Delivery

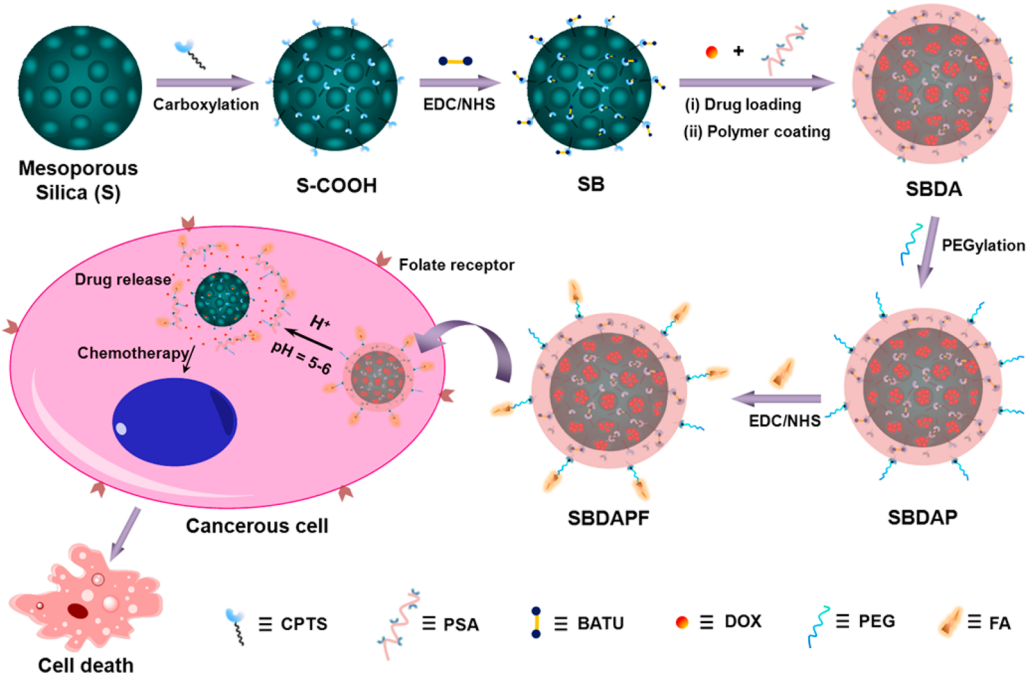

clearance of DDSs during the circulation, whereas in situ polymerization approaches require harsh reaction conditions and generate probably the agglomeration of the nanoparticles. Moreover, these two strategies are not suitable for constructing versatile DDSs that allow drug releasing at the appropriate time and site. Recently, a new so-called "programmed packing" manner was proposed to design versatile DDSs for tumor-activated targeting drug delivery.[28] In this manner, cyclodextrin was first grafted to the MSNs surface through disulfide bonding. Then some functional units, including tumor-targeting peptides and polyanion protection layer, were successively conjugated with nanoparticles. Using the "programmed packing" strategy, the assembled functional units can perform well their respective functions at desired time as well as at appropriate sites. Nevertheless, versatile envelope-type DDSs constructed by the programmed packing manner have been rarely reported.

Inspired from the concept of programmed packing, here, we designed and constructed a multifunctional pH-sensitive envelope-type mesoporous silica nanocontainer with diverse functional components, such as tumor-targeting units to mediate specific uptake by cancer cells, polymer coating layer to avoid the nonspecific uptake, and inhibit the premature drug release, and pH-sensitive linkers to achieve the acid-responsive drug release at desired time and site. Scheme 1 demonstrates the schematic illustration of construction of this nanocontainer and its application for cancer cell targeting and intracellular pH-triggered drug releasing. An acid-labile acetal linker 3,9-bis(3-aminopropyl)-2,4,8,10-tetraoxaspiro[5.5]undecane (BATU) is grafted to mesoporous silica surface modified with carboxyl groups via the EDC/NHS process. Then an antineoplastic drug DOX is filled into the mesopores of functional mesoporous silica with the surface-coated with poly(*N*-succinimidyl acrylate) (PSA). The polymer PSA behaves as a dual-purpose entity that not only guards the drug payload from premature release but also acts as a cross-linking agent for the immobilization of other functional components on nanoparticles surface. Moreover, as for cancer therapy, the resulting nanocontainers are successively decorated with biocompatible poly(ethylene glycol) (PEG) and floic acid (FA). The PEG, as a protection layer, can decrease the nonspecific uptake resulting from an inhibition of the interaction of the nanocontainers with the healthy cells surface,[29] and FA, as a cancer-targeting unit, can enhance the uptake of nanocontainers by the cancer cells via ligand-mediated cell adhesion.[30] After the nanocontainers arrive at tumor tissues, FA on outer layer can selectively conjugate with folate receptor of cancer cells, resulting in the tumor-specific cell uptake. Thereafter, the polymer coating layer can be removed due to the breakage of acetal bonds triggered by an acidic pH inside the cancer cells, and then the drug payload can be quickly released from the nanocontainer.[22,31] Consequently, we hypothesize that this versatile envelope-type mesoporous silica nanocontainer (SBDAPF) is a potential intracellular pH-responsive controlled release system for targeted drug delivery.

EXPERIMENTAL SECTION

Reagents and Materials. [3-(Dimethylamino)propyl]-3-ethylcarbodiimide hydrochloride (EDC), *N*-(trimethoxysilylpropyl)-ethylenediamine triacetic acid (CPTS), poly(acrylic acid) (PAA), and *N*-cetyltrimethylammonium bromide (CTAB) were obtained from Alfa Aesar. 3,9-Bis(3-aminopropyl)-2,4,8,10-tetraoxaspiro[5.5]-undecane (BATU), *N*-succinimidyl acrylate, and 1,11-diaminoundecane were obtained from TCI (Shanghai, China). Poly(ethylene glycol) diamine (M_w = 3.4 × 10^3), 3-[4,5-dimethylthialzol-2-yl]-2,5-diphenyltetrazolium bromide (MTT), and 2,2′-azobis(2-methylpropionitrile) (AIBN, 98%) were obtained from Sigma-Aldrich. Lysotracker Blue was purchased from Invitrogen. Hoechst 33342, folic acid, doxorubicin hydrochloride (DOX), tris(hydroxymethyl)-aminomethane hydrochloride (Tris), and *N*-hydroxysuccinimide (NHS, 98%) were obtained from Dingguo reagent company. Sodium hydroxide (NaOH), HCl solution (37%), benzene, tetrahydrofuran (THF), anhydrous toluene, and tetraethylorthosilicate (TEOS, 28%) were purchased from Xilong reagent company. All the chemicals were used without further purification. HepG2 cells (human liver

DOI: 10.1021/acsami.5b04684
ACS Appl. Mater. Interfaces 2015, 7, 17399−17407

hepatocellular carcinoma cells) and L02 cells (human hepatocyte L02 cells) were purchased from the American Type Culture Collection (Manassas, VA).

Characterization. Transmission electron microscopy (TEM) images were obtained from a JEOL 3010 microscope with accelerating voltage of 100 kV. N_2 adsorption−desorption isotherm was obtained at −196 °C on a Micromeritics ASAP 2010 sorptometer. UV−vis spectra were obtained using a UV-800. Fourier transform infrared (FTIR) spectra were collected from TENSOR 27 spectrometer using KBr pellets. Small-angle powder X-ray diffraction pattern (XRD) of the mesoporous silica nanomaterials was collected in a Scintag XDS-2000 powder diffractometer. GPC analysis was performed on a Shimadzu LC-10AD. The thermal gravimetric analysis (TGA) was performed on a TG 209 F1 (NETZSCH) instrument with a heating rate of 10 °C min^{-1}. All fluorescence spectra were recorded on a Hitachi F4500 FL spectrophotometer. Confocal laser scanning microscopy (CLSM) images were collected on a Fluoview FV500, Olympus. Flow cytometry analyses were performed using a FACSCalibur flow cytometer. The MTT assays were carried out on a Benchmark Plus, Biorad Instruments, Inc.

Synthesis of Poly(*N*-Succinimidyl Acrylate) (PSA). A mixture of *N*-succinimidyl acrylate (0.22 g, 1.3 mmol) and AIBN (2 mg) in benzene (10 mL) was reacted for 24 h at 60 °C.[32] After the reaction solution was cooled down to room temperature, a white precipitate was observed. The resulting precipitate was then separated by centrifugation and washed with tetrahydrofuran (2 mL). The purified white solid was dried in vacuo at 60 °C for 24 h to yield the PSA.

Preparation of SB. Mesoporous silica (S) was first obtained by a base-catalyzed sol−gel process. In brief, *N*-cetyltrimethylammonium bromide (CTAB, 0.5 g) as surfactant template was dissolved in distilled water (240 mL). NaOH (2.00 M, 1.75 mL) was then added to CTAB solution, followed by regulating the mixed solution temperature to 60 °C. TEOS (2.50 mL) was added dropwise to the mixed solution under sharp stirring condition. After hydrolysis reaction for 2 h, a white precipitate S was formed, followed by separating by centrifugation and washing with ethanol. The obtained S particles were subsequently modified with carboxyl groups (S-COOH) via the hydrolyzation of *N*-(trimethoxysilylpropyl)ethylenediamine triacetic acid (CPTS) on nanoparticles surface. Briefly, S particles (0.2 g) were dispersed in anhydrous toluene (50 mL) to which 0.3 mL of CPTS was added while continuously stirring at 80 °C for 20 h. Then, the resulting particles were collected and rinsed with ethanol to gain crude S-COOH. Finally, the S-COOH particles were refluxed in hot acetone for 48 h to remove template CTAB.

To obtain the pH sensitive property, an acid-cleavable linker, 3,9-bis(3-aminopropyl)-2,4,8,10-tetraoxaspiro[5.5]undecane (BATU),[22] was grafted to the mesoporous silica surface. In brief, S-COOH particles (20 mg) were suspended in 1 mL of DMF containing EDC (12 mg) and NHS (5 mg), and then BATU (65 mg) was added. After the mixture was reacted for 8 h in shaker, the suspended particles were collected and denoted as SB. As a control, a noncleavable control 1,11-diaminoundecane linker instead of BATU was immobilized on the nanoparticles surface via the same approach to yield the SU particles.[31,33]

Drug Loading. SB particles were added into DOX solution and incubated in shaker at room temperature overnight. DOX molecules in solution can diffuse into the pore channels. The DOX-loaded SB was separated by centrifugation and rinsed with water to get rid of the redundant DOX. To inhibit the DOX release from pore channels, DOX-loaded SB (15 mg) was treated with of PSA (5 mg) in 1 mL of DMF for 8 h at room temperature. Finally, the resulting particles were respectively washed with DMF, ethanol, and water, and dried in vacuo at 60 °C to yield SBDA. The amount of DOX loaded into SBDA was estimated by fluorescence intensity at 560 nm (λ_{ex} = 488 nm). Loading content = (initial weight of DOX − supernatant weight of DOX)/weight of particles × 100%.

In Vitro Test of Drug Release. A sample of SBDA (5 mg) was suspended in 5 mL of acetate buffer or PBS buffer with various pH values (pH 2.0, 5.0, 6.5, and 7.4). Aliquots were drawn from the suspension solution at certain intervals and the released DOX molecules were estimated by testing the fluorescence intensity of supernatant solution (λ_{ex} = 488 nm, λ_{em} = 560 nm).

Preparation of SBDAPF. To improve colloidal stability and water dispersibility of nanocontainers for subsequent cell experiments, initially, SBDA particles (2.0 mL, 1.0 mg mL^{-1}) were decorated with poly(ethylene glycol) diamine (M_w = 3.4 × 10^3) by the reaction between amine group with the immobilized PSA to give rise to the SBDAP particles. Then, folic acid (0.1 mg) was dissolved in the SBDAP suspension (1 mL, 1.0 mg mL^{-1}). Also, EDC (0.5 mg) and NHS (0.5 mg) were successively added to the mixture solution. The amide formation reaction was allowed overnight. The reacted product was separated and purified to yield the SBDAPF particles.

Flow Cytometry. HepG2 or L02 cells (10^5 cells/well) were incubated in cell culture medium with 10% fetal calf serum (FBS) under 5% CO_2 atmosphere at 37 °C for 24 h. The HepG2 cells were rinsed with washing buffer (1 mL) and then treated with different concentrations (0, 1, 5, 10, 20, 50, and 100 μg mL^{-1}) of SBDAPF or SBDAP for 1 h at 4 °C. They were again washed to remove the physically adsorbed nanoparticles, and then incubated with trypsin (500 μL, 0.05%)/EDTA (0.53 mM) in Hank's balanced salt solution at 37 °C. After 10 min of incubation, the cells were placed in PBS buffer for the flow cytometric assay. As a control, the L02 cells were coincubated with SBDAPF (20 μg mL^{-1}) at 4 °C for 1 h. After the same treatment procedure, the L02 cells were dispersed in PBS buffer for the flow cytometric assay.

In addition, to quantify the SBDAPF internalized into the cells, HepG2 and L02 cells were respectively treated with SBDAPF nanocontainers at 37 °C. After 3 h of incubation, they were suspended in PBS buffer for the flow cytometric analysis. Also, SBDAP was used as a negative control and incubated with HepG2 and L02 cells, respectively.

Confocal Fluorescence Imaging. HepG2 or L02 cells were incubated in cell culture medium (2 mL) containing 10% FBS in a humidified atmosphere with 5% CO_2 at 37 °C for 24 h. Thereafter, SBDAPF (20 μg mL^{-1}) was added, and the cells were incubated for another 3 h at 37 °C. For the colocalization experiments, Lysotracker Blue (1 μL) was used for selective staining of the late endosomes and lysosomes of living cells. After the medium was removed and they were washed with PBS buffer (2 mL, pH 7.4), the HepG2 and L02 cells were, respectively, observed by using CLSM.

To demonstrate the intracellular drug release, HepG2 cells were incubated with SBDAPF (100 μg mL^{-1}) for 6 h at 37 °C. Also, HepG2 cells were incubated with a low concentration of SBDAPF (50 μg mL^{-1}) for a short time (3 h). For the colocalization study, Hoechst 33342 (1.0 mg mL^{-1}) was used for specific staining of the cell nucleus. After the medium was removed and the cells were washed wash with PBS buffer (2 mL, pH 7.4), HepG2 cells were observed by CLSM. As a control, the SUDAPF-treated and untreated HepG2 cells were also investigated by the same process.

Cell Viability Assay. MTT assay was performed to investigate the cytotoxicity of different nanoparticles to HepG2 or L02 cells. HepG2 cells in a 96-well plate (5 × 10^4 cells/well) were incubated with various concentrations of free DOX, SBDAPF, SUDAPF, SBAPF, and SBDAP for 24 h. MTT solution (60 μL, 0.5 mg mL^{-1}) was subsequently added to each well, and the cells were further incubated for 4 h. The MTT medium was then removed and DMSO (150 μL) was added to dissolve the formed formazan violet crystals. The absorbance of formazan in DMSO solution was detected by a microplate reader at 570 nm. The cell viability was calculated by the equation

$$\text{viability} = (A_{\text{treated}}/A_{\text{control}}) \times 100\%$$

where A_{treated} was obtained from the cells treated by nanoparticles and A_{control} was obtained from the cells without any treatments. The viability of L02 cells after being incubated with SBDAP or SBDAPF was also estimated by the same process.

RESULTS AND DISCUSSION

Preparation and Characterization of SBA Nanocontainers. The synthesis process of SBA is presented in

DOI: 10.1021/acsami.5b04684
ACS Appl. Mater. Interfaces 2015, 7, 17399−17407

Scheme S1. The mesoporous silica was first synthesized by using a previously reported procedure with TEOS as a silica precursor, CTAB as a surfactant template and NaOH as a catalyst. The as-prepared nanoparticles were modified with *N*-(trimethoxysilylpropyl)ethylenediamine triacetic acid to gain crude functional mesoporous silica-modified with carboxyl groups (S-COOH). CTAB was then extracted from mesopores by refluxing in methanol containing HCl. The purified S-COOH was characterized by TEM, SEM, XRD, N_2 adsorption−desorption measurements, ζ-potential measurements, and FT-IR spectra. SEM and TEM images of S-COOH showed an average diameter of ∼100 nm and a typical channel-like mesostructure (Figure 1A and C). The XRD

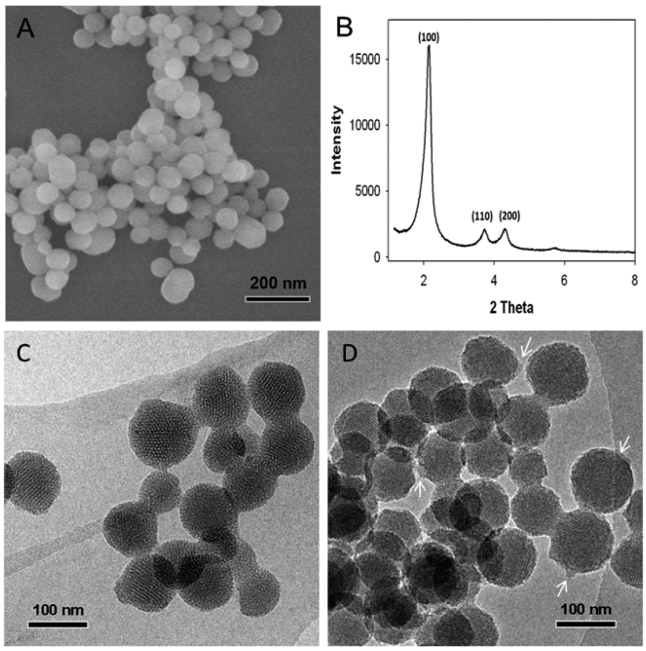

Figure 1. (A) SEM image of S-COOH and (B) low-angle XRD pattern of S-COOH. TEM images of S-COOH (C) and SBA (D).

pattern of S-COOH further indicated a uniform, well-defined pore channel structure (Figure 1B). Furthermore, the N_2 adsorption−desorption isotherm of the S-COOH demonstrated a typical of a type IV curve with a surface area of 817.6 m^2 g^{-1}, a pore volume of 0.69 cm^3 g^{-1}, and a narrow pore size distribution (2.72 nm) (Figure S1). Subsequently, the obtained S-COOH was decorated with an acetal linker 3,9-bis(3-aminopropyl)-2,4,8,10-tetraoxaspiro[5.5] undecane (BATU) by the amide formation reaction to produce SB particles. The increased ζ potential from −36.4.0 to 21.7 mV (Table S1) suggested that BATU had been covalently grafted to the surface of S-COOH. Meanwhile, from the FT-IR spectra, we can see that the S-COOH has an absorption peak at wavenumber of 1645 cm^{-1} (Figure S2), which is indicative of the C═O stretching vibrations of carboxyl groups. After BATU immobilizing, it exhibits two absorption peaks at 1575 and 1478 cm^{-1} that are respectively assigned to the asymmetric N−H bending vibrations and the C−N stretching bands. This result further confirmed the successful immobilization of BATU linker. The obtained SB particles showed good water dispersibility (Figure S3 and Table S2). The amount of BATU grafted to SB particles was estimated by TGA analysis. As demonstrated in Figure 2, the weight loss values of S-

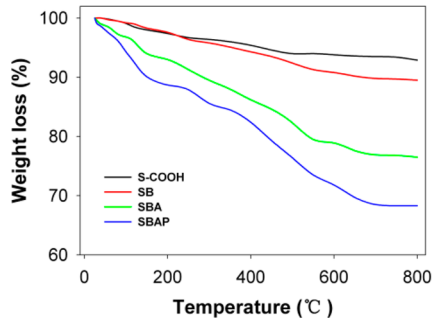

Figure 2. TGA curves of various nanoparticles such as S-COOH, SB, SBA, and SBAP.

COOH and SB, after heating them to 800 °C under N_2 atmosphere, were 7.1% and 10.5%, respectively. The percentage of BATU on the nanoparticles was thus determined to be about 3.4%. As a control, a noncleavable linker 1,11-diaminoundecane instead of BATU was used to form the SU particles.

In our design, polymer was employed as a pore blockage for inhibiting the release of entrapped drug molecules. The polymer PSA was thus synthesized via homopolymerization of *N*-succinimidyl acrylate. The molecular weight of PSA (as poly(acrylic acid) (PAA)) was estimated by GPC analysis after complete hydrolysis of PSA by a simple treatment with HCl solution.[32] The M_w of PAA was 103 000, and the degree of polymerization was 1430. Then the PSA was wrapped on the surface of SB by mixing the polymer and SB particles in DMF. After the coating process, FT-IR spectra of resulting particles (SBA) had strong absorption peaks at the wavenumbers of 2916 and 2847 cm^{-1}, which were assigned to the asymmetric C−H stretching vibrations. Moreover, TEM image of SBA display a thin polymeric shell (Figure 1D, white arrows), which is absent on uncoated nanoparticles, indicating the successful functionalization of PSA.[34] The DLS result of SBA demonstrated an obvious increase of hydrodynamic size by comparison with that of SB particles (Figure S3 and Table S2). The DLS and TEM data also prove that the polymer coating do not cause the agglomeration of the nanoparticles into the micrometer-scale aggregates. The percentage of PSA wrapped on SBA surface was calculated to be 13% via TGA analysis.

Drug Loading and Release. To investigate the pH-responsive controlled drug release, the anticancer drug DOX was selected as a model drug molecule and filled into pore channels of SB prior to the polymer coating process. The DOX-loaded SB was then treated with polymer PSA to seal the pore mouths and inhibit the release of loaded DOX. The obtained DOX-loaded SBA (SBDA) exhibited a characteristic absorption at 488 nm corresponding to DOX, whereas DOX-unloaded SBA showed no absorption at 380−580 nm (Figure S4). This photophysical property of SBDA provided a credible evidence for the stable encapsulation of DOX. The DOX loading content was about 5.6%, estimated by the fluorescence emission intensity at 560 nm (λ_{ex} = 488 nm). Meanwhile, DOX was also loaded into the control SU particles by the same process. Therefore, the nonresponsive SUDA particles were obtained. The DOX loading content in SUDA particles was approximately 5.9%.

To test the acid-sensitive uncapping of SBDA nanocontainers, we first investigated if treatment of the SBDA with acid resulted in the DOX release. In these experiments,

DOI: 10.1021/acsami.5b04684
ACS Appl. Mater. Interfaces 2015, 7, 17399−17407

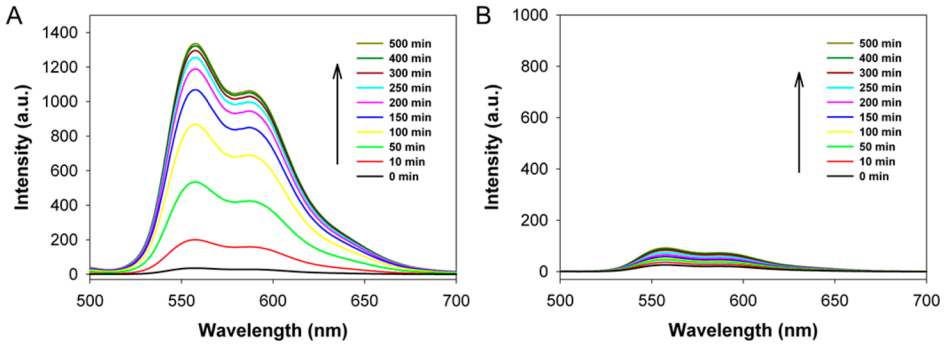

Figure 3. Fluorescence emission of released DOX from SBDA (A) and SUDA (B) in PBS buffer solution (pH 5.0).

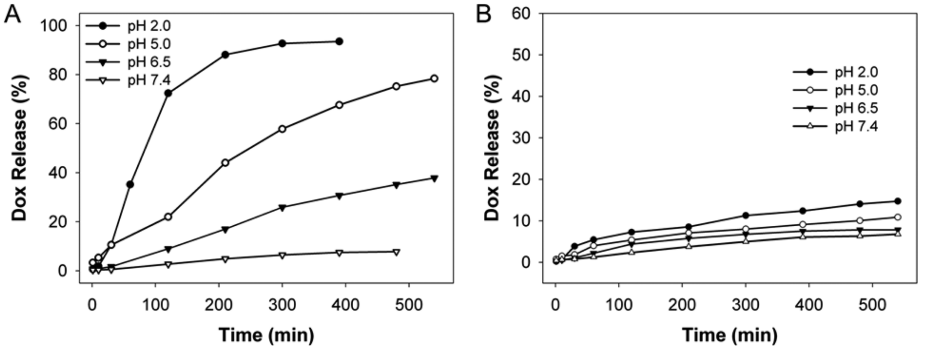

Figure 4. pH-responsive release of DOX from SBDA (A) and SUDA (B) in buffer with different pH values.

SBDA particles were incubated with PBS buffer (pH 5.0), and fluorescence emissions in the supernatant solution (λ_{ex} = 488 nm, λ_{em} = 560 nm) were obtained at various time points. As demonstrated in Figure 3A, the fluorescence emission in supernatant increased as a result of the release of the loaded DOX, reaching a plateau within 180 min. As expected, a nominal increase in fluorescence (no DOX release) was observed in the case of SUDA (Figure 3B). In addition, treatment of free DOX (50 μM) with PBS buffer (pH 5.0) has no effect on the fluorescence emission of DOX (Figure S5), further suggesting that the observed increase in fluorescence of supernatant solution was due to acid-responsive cleavage of the acetal bond and subsequent DOX release. Moreover, we compared the DOX release from SBDA and SUDA particles after being incubated with different pH value solution. Results show that within 180 min of incubation, a pH-dependent DOX release was observed when the SBDA particles were used (Figure S6). In contrast, a negligible DOX release from SUDA particle was noted at different pH values.

To further show the pH-responsive drug releasing behavior, in vitro release experiments were carried out at various pH values (pH 2.0, 5.0, 6.5, and 7.4). SBDA particles (5 mg) were first suspended in PBS buffer (pH 7.4). At desired time intervals, the supernatant solution was then collected to calculate the accumulative release amount of DOX. As shown in Figure 4, only 5.8% DOX payload was released at pH 7.4 after 500 min, which was an insignificant DOX release. The low premature release behavior exhibited the excellent blocking performance of polymer-coating mesoporous silica systems. Subsequently, the pH values of three samples were adjusted to pH 6.5, 5.0, and 2.0, respectively. The release of DOX was observed immediately after the change of pH values of the solution. The cumulative amount of DOX is up to 37.9% at pH 6.5, 78.4% at pH 5.0, and 93.5% at pH 2.0. However, there is only 7.4% of drug release from the control SUDA particles at pH 2.0, indicating the pH-triggered DOX release property was attributed to the use of acid-sensitive acetal bonds. These results confirmed that drug payload had been strongly inhibited in pore channels blocked with polymer at physiological pH, but the entrapped drug had been rapidly released at acidic pH. In a word, the polymer coating layer had played the role of pore switch in the drug release via a pH-responsive "open-closed" mechanism.

Specific Binding and Internalization of SBDAPF Nanocontainers. For cancer therapy, the potential side effects of nanocontainers should be considered. To reduce the toxic side effects, many targeted DDSs have been developed by introducing the targeting components. FA, as a universal targeting unit, can anchor selectively to the cancer cells via ligand-mediated cell adhesion. In the cellular level, more than 40% of human cancer cells overexpress folate receptors, whereas normal tissues and cells have no folate receptor expression.[35] To endow these nanocontainers with high specific recognition capability, thus, FA was grafted to the mesoporous nanocontainers (Scheme S1). For this, SBA containers was first functionalized with biocompatible poly(ethylene glycol) diamine by the reaction between PSA immobilized on the particles and amine groups to improve colloidal stability and avoid nonspecific cell uptake of nanocontainers. The results of DLS measurements confirmed the successful functionalization (Figure S3 and Table S2). From Figure 2, the weight percentage of immobilized poly(ethylene glycol) diamine was calculated to be approximately 7.5%. After that, folic acid was anchored onto the surface of PEGylated SBDA particles (SBDAP) by the EDC/NHS process to finally synthesize the SBDAPF nanocontainer.

Subsequently, the targeting efficiency of SBDAPF was tested. To avoid the nonspecific cell uptake of nanoparticles during

DOI: 10.1021/acsami.5b04684
ACS Appl. Mater. Interfaces 2015, 7, 17399−17407

testing, the binding experiments were performed at 4 °C.[36] Then the specific binding ability of SBDAPF to the targeted HepG2 cells was investigated by using flow cytometry. As demonstrated in Figure 5A, a great fluorescence shift was

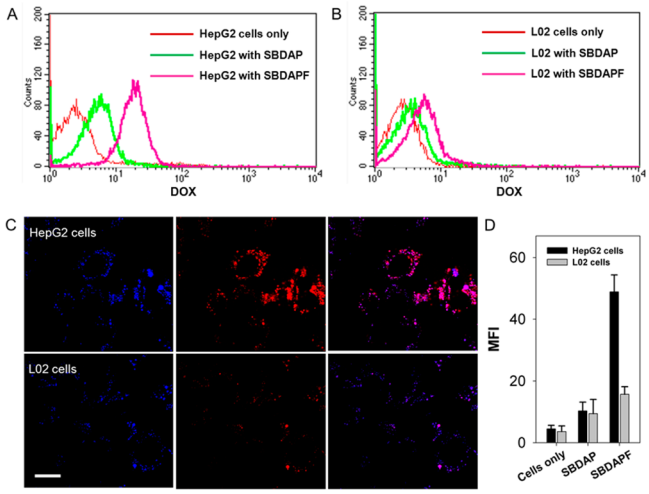

Figure 5. Flow cytometric analysis to assess the specific binding ability of SBDAP and SBDAPF toward HepG2 cells (A) and L02 cells (B) for 1 h at 4 °C. (C) CLSM images of the colocalization of SBDAPF (red) after incubation with HepG2 and L02 cells at 37 °C for 3 h. Lysotracker Blue (blue) was employed to specifically stain the late endosomes and lysosomes in living cells. The scale bar is 20 μm. (D) Flow cytometric comparison of cell uptake of different nanoparticles (20 μg mL^{-1}). MFI represents the mean fluorescence emission intensity of DOX in cells.

observed for HepG2 cells after being incubated with SBDAPF, indicating that the SBDAPF nanocontainers were successfully bound on the surface of the cells. In contrast, only a negligible fluorescence change was noted for the SBDAP-treated HepG2 cells due to the lack of folate ligand. Moreover, no significant fluorescence change was obtained for L02 cells (normal cells with low expression level of folate receptors) after incubation with SBDAPF and SBDAP (Figure 5B), respectively. These results provided the adequate evidence for the specific recognition of the SBDAPF nanocontainers to targeted HepG2 cells. In addition, the effect of nanocontainer concentrations on the binding efficiency was also studied. To do this, HepG2 cells were incubated with serial concentrations of SBDAPF or SBDAP at 4 °C for 1 h. From Figure S7, the fluorescence signal of SBDAPF-treated HepG2 cells obviously increased with increasing the SBDAPF concentration, suggesting that the total amount of SBDAPF bound on HepG2 cells is remained increase. A saturated fluorescence signal was achieved when the concentration of SBDAPF reached 20 μg mL^{-1}. This result verifies that the number of SBDAPF bound on HepG2 cells is related to the total amount of folate acceptors on cells. In contrast, HepG2 cells treated with SBDAP showed a low fluorescence enhancement, implying that a small quantity of SBDAP was adhered to HepG2 cells by the unspecific adsorption.

The highly specific binding efficiency of SBDAPF to HepG2 cells is important to enhance the particle uptake. To prove this, we carried out flow cytometry experiments to test the amount of cellular uptake of different nanoparticles. As demonstrated in Figure 5D, the mean fluorescence intensity (MFI) values of HepG2 cells treated with SBDAPF and SBDAP particles at 37 °C for 3 h were 48.9 and 9.6 (a.u.), respectively. This study showed that HepG2 cells could internalize ~5 times more SBDAPF than SBDAP. On the contrary, there was no obvious increase of MFI values in L02 cells treated with SBDAPF compared with SBDAP. Furthermore, we characterized the internalization procedure of SBDAPF by using confocal laser scanning microscopy (CLSM). According to the previously reported literatures, most of nanocontainers were internalized by the cellular endocytosis, that is, the nanocontainers entered into the early endosomes, then into the late endosomes, and finally merged with lysosomes of cells.[11,30,33,37] In the cell uptake experiments, thus, Lysotracker Blue was employed to selectively stain the late endosomes and lysosomes of living cells after being incubated with SBDAPF (20 μg mL^{-1}) for 3 h. CLSM images of HepG2 cells demonstrated the strong DOX fluorescence (red), which overlapped with fluorescence of Lysotracker Blue, suggesting that SBDAPF was located in the late endosomes or lysosomes in cells (Figure 5C). In contrast, only a weak DOX fluorescence was seen in L02 cells. These results confirmed that the existence of folate acceptors on cells was a key factor for the enhanced cell uptake of nanocontainers, and SBDAPF could be selectively internalized into HepG2 cells.

Intracellular Drug Release of SBDAPF Nanocontainers. As we know, both endosomes and lysosomes are slightly acidic intracellular compartments.[12,38,39] After being internalized into cells, SBDAPF nanocontainers can release the entrapped DOX into the cytoplasm triggered by an acidic pH signal at the late endosomes/lysosomes. It is well-known that the active site of DOX is the nuclei of cells, where DOX can anchor to double-stranded DNA to induce cell death.[40] Therefore, the intracellular release and distribution of DOX payload in HepG2 cells were investigated by CLSM. From Figure S8, after being incubated with SBDAPF (50 μg mL^{-1}) for a short time (3 h), HepG2 cells displayed a low accumulation of nanocontainers only in the cytoplasm. Also the HepG2 cells incubated with nonresponsive SUDAPF particles had no DOX release under the same conditions. This result indicated that the drug release was probably delayed in endosomes or lysosomes and the traffic process even though some nanocontainers were internalized into cells within 3 h. To confirm this, HepG2 cells were further incubated with SBDAPF nanocontainers (100 μg mL^{-1}) for 6 h. CLSM images demonstrated an obvious fluorescence of DOX in both the cytoplasm and the nucleus of cells (Figure 6), thus suggesting that DOX payload was released and finally trafficked into the cell nucleus. However, there is still no distribution of DOX in the cell nuclei of HepG2 cells after treatment with SUDAPF particles owing to the lack of acid-labile acetal linker. Moreover, untreated HepG2 cells had no fluorescence signal in DOX channel, which availably eliminated the possible interference of autofluorescence. All the above results indicate that the drug delivery mechanism involves the specific cell uptake of SBDAPF nanocontainers, followed by the hydrolysis of the acetal bond in the slightly acidic endosomes or lysosomes in cells, and the subsequent the delivery of drug payload from pore channels to the nuclei of cells.

Cytotoxicity of SBDAPF Nanocontainers. To estimate the targeting cell killing efficacy of SBDAPF nanocontainers, MTT assay was performed to quantify the viability of cells treated with nanocontainers. Figure 7 showed the viability of HepG2 cells after being incubated with a series of concentrations of SBAPF, free DOX, SBDAPF, and SUDAPF

DOI: 10.1021/acsami.5b04684
ACS Appl. Mater. Interfaces 2015, 7, 17399−17407

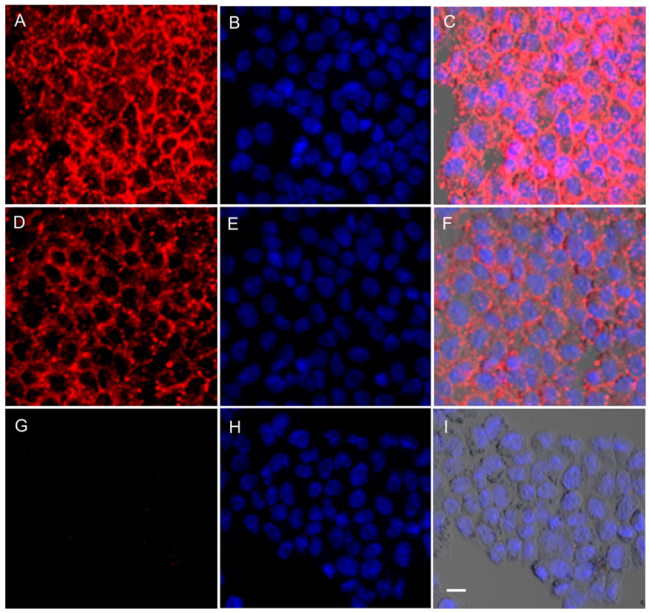

Figure 6. CLSM images of HepG2 cells treated with SBDAPF (A–C) and SUDAPF (D–F) nanocontainers (100 μg mL^{-1}) at 37 °C for 6 h, respectively. The untreated HepG2 cells with nanoparticles was as negative control (G–I). The red was regarded as the fluorescence of DOX (A, D, G). Hoechst 33342 (blue) was used to stain the cell nucleus (B, E, H). The CLSM images were overlapped (C, F, I). The scale bar is 20 μm.

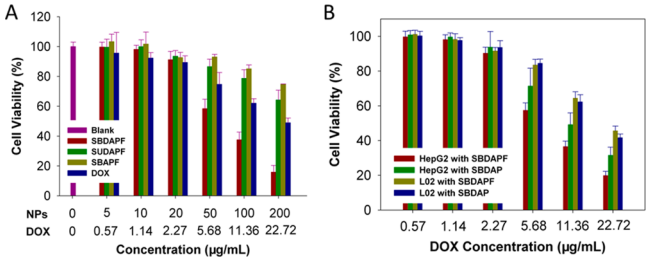

Figure 7. (A) Viability of HepG2 cells after being treated with various concentrations of free DOX or nanocontainers. (B) Cytotoxicity of SBDAPF and SBDAP particles incubated with HepG2 cells and L02 cells for 24 h.

for 24 h, respectively. HepG2 cells treated with DOX-unloaded SBAPF particles showed high viability (above 80%), indicating that the nanocontainers had a good biocompatibility. In contrast, the cytotoxicity of SBDAPF (DOX-loaded nanocontainers) was significant. Although both SBDAPF and free DOX exhibited dose-dependent toxicity to the HepG2 cells, SBDAPF had much stronger toxicity than free DOX at the same DOX content, implying that entrapped DOX into nanocontainer enhanced the killing efficacy of DOX. This cytotoxicity enhancement effect of SBDAPF results from the increased cell uptake of nanocontainers via folate-mediated endocytosis compared with the diffusion of free DOX. However, nonresponsive SUDAPF particles had no obvious cytotoxic effect on HepG2 cells at the same conditions. This is because the entrapped DOX into SUDAPF particles cannot be effectively released from mesoporous channels as a result of the lack of acid-sensitive linker. To further investigate the effect of folate molecules on the targeted cancer therapy, HepG2 cells were incubated with nontargeting SBDAP particles. From Figure 7B, the viability of SBDAP-treated HepG2 cells was higher than that of SBDAPF-treated cells, suggesting that targeting unit folate molecules were significantly important for HepG2 cell killing. In addition, viability of control L02 cells was also investigated in the presence of SBDAPF or SBDAP particles. As a result, L02 cells after being incubated with SBDAPF or SBDAP particles showed the higher viability than HepG2 cells. These results prove that the constructed SBDAPF has a good killing efficacy to targeted cells and a significant benefit to decrease the toxic side effects to normal or healthy cells.

CONCLUSIONS

In summary, we designed and constructed a novel multifunctional envelope-type mesoporous silica nanocontainer (SBDAPF) with folate-mediated cancer cell uptake and intracellular pH-responsive controlled drug release properties. The polymer coating layer effectively blocked the pore channels and prevented the entrapped antineoplastic drug DOX from premature release at physiological pH. Under the acidic conditions, DOX could be rapidly released as a result of the disassociation of polymer coating layer. Importantly, the massive drug molecules were able to be released in mild acidic conditions (pH = 5–6). In vitro experiments indicated that SBDAPF acquired the ability of the targeting accumulation within cancer cells and showed the enhanced cancer cell killing efficacy. We believe that this versatile drug delivery system has great potential applications in the field of cancer therapy.

ASSOCIATED CONTENT

Supporting Information

The Supporting Information is available free of charge on the ACS Publications website at DOI: 10.1021/acsami.5b04684.

ζ potential and FT-IR spectra of the synthesized nanoparticles, nitrogen adsorption–desorption isotherm, DLS measurements, pore size distribution, UV–vis spectra, fluorescence spectra, and CLSM images (PDF)

AUTHOR INFORMATION

Corresponding Authors

*E-mail: yangkenhm@163.com.
*E-mail: lijming0901@sina.com.

Notes

The authors declare no competing financial interest.

ACKNOWLEDGMENTS

We are grateful to the financial support from the Construct Program of the Key Discipline in Hunan Province and the Research Foundation of Education Bureau of Hunan Province (13C1120).

REFERENCES

(1) Peer, D.; Karp, J. M.; Hong, S.; Farokhzad, O. C.; Margalit, R.; Langer, R. Nanocarriers as an Emerging Platform for Cancer Therapy. *Nat. Nanotechnol.* **2007**, *2*, 751–760.
(2) Park, K. Controlled Drug Delivery Systems: Past Forward and Future Back. *J. Controlled Release* **2014**, *190*, 3–8.
(3) Tang, F.; Li, L.; Chen, D. Mesoporous Silica Nanoparticles: Synthesis, Biocompatibility and Drug Delivery. *Adv. Mater.* **2012**, *24*, 1504–1534.
(4) Ashley, C. E.; Carnes, E. C.; Phillips, G. K.; Padilla, D.; Durfee, P. N.; Brown, P. A.; Hanna, T. N.; Liu, J.; Phillips, B.; Carter, M. B.; Carroll, N. J.; Jiang, X.; Dunphy, D. R.; Willman, C. L.; Petsev, D. N.; Evans, D. G.; Parikh, A. N.; Chackerian, B.; Wharton, W.; Peabody, D.

DOI: 10.1021/acsami.5b04684
ACS Appl. Mater. Interfaces 2015, 7, 17399–17407

S.; Brinker, C. J. The Targeted Delivery of Multicomponent Cargos to Cancer Cells by Nanoporous Particle-Supported Lipid Bilayers. *Nat. Mater.* **2011**, *10*, 389−397.
(5) Yang, P.; Gai, S.; Lin, J. Functionalized Mesoporous Silica Materials for Controlled Drug Delivery. *Chem. Soc. Rev.* **2012**, *41*, 3679−3698.
(6) Li, Z.; Barnes, J. C.; Bosoy, A.; Stoddart, J. F.; Zink, J. I. Mesoporous Silica Nanoparticles in Biomedical Applications. *Chem. Soc. Rev.* **2012**, *41*, 2590−2605.
(7) Li, M. H.; Yan, Y.; Teh, C.; Korzh, V.; Zhao, Y. L. NIR Triggered Drug Release from Switchable Rotaxane-Functionalized Silica-Covered Au Nanorods. *Chem. Commun.* **2014**, *50*, 9745−9748.
(8) Fedoryshin, L. L.; Tavares, A. J.; Petryayeva, E.; Doughan, S.; Krull, U. J. Near-Infrared-Triggered Anticancer Drug Release from Upconverting Nanoparticles. *ACS Appl. Mater. Interfaces* **2014**, *6*, 13600−13606.
(9) Yu, Z. Z.; Li, N.; Zheng, P. P.; Pan, W.; Tang, B. Temperature-Responsive DNA-Gated Nanocarriers for Intracellular Controlled Release. *Chem. Commun.* **2014**, *50*, 3494−3497.
(10) Luo, Z.; Ding, X. W.; Hu, Y.; Wu, S. J.; Xiang, Y.; Zeng, Y. F.; Zhang, B. L.; Yan, H.; Zhang, H. C.; Zhu, L. L.; Liu, J. J.; Li, J. H.; Cai, K. Y.; Zhao, Y. L. Engineering a Hollow Nanocontainer Platform with Multifunctional Molecular Machines for Tumor-Targeted Therapy in Vitro and in Vivo. *ACS Nano* **2013**, *7*, 10271−10284.
(11) Dai, L. L.; Li, J. H.; Zhang, B. L.; Liu, J. J.; Luo, Z.; Cai, K. Y. Redox-Responsive Nanocarrier Based on Heparin End-Capped Mesoporous Silica Nanoparticles for Targeted Tumor Therapy in Vitro and in Vivo. *Langmuir* **2014**, *30*, 7867−7877.
(12) Muhammad, F.; Wang, A. F.; Guo, M. Y.; Zhao, J. Y.; Qi, W. X.; Guo, Y. J.; Gu, J. K.; Zhu, G. S. pH Dictates the Release of Hydrophobic Drug Cocktail from Mesoporous Nanoarchitecture. *ACS Appl. Mater. Interfaces* **2013**, *5*, 11828−11835.
(13) Tan, L.; Yang, M.-Y.; Wu, H.-X.; Tang, Z.-W.; Xiao, J.-Y.; Liu, C.-J.; Zhuo, R.-X. Glucose- and pH-Responsive Nanogated Ensemble Based on Polymeric Network Capped Mesoporous Silica. *ACS Appl. Mater. Interfaces* **2015**, *7*, 6310−6316.
(14) Zhang, G. L.; Yang, M. L.; Cai, D. Q.; Zheng, K.; Zhang, X.; Wu, L. F.; Wu, Z. Y. Composite of Functional Mesoporous Silica and DNA: An Enzyme-Responsive Controlled Release Drug Carrier System. *ACS Appl. Mater. Interfaces* **2014**, *6*, 8042−8047.
(15) Meng, H.; Xue, M.; Xia, T.; Zhao, Y. L.; Tamanoi, F.; Stoddart, J. F.; Zink, J. I.; Nel, A. E. Autonomous in Vitro Anticancer Drug Release from Mesoporous Silica Nanoparticles by pH-Sensitive Nanovalves. *J. Am. Chem. Soc.* **2010**, *132*, 12690−12697.
(16) Zhang, Q.; Liu, F.; Nguyen, K. T.; Ma, X.; Wang, X. J.; Xing, B. G.; Zhao, Y. L. Multifunctional Mesoporous Silica Nanoparticles for Cancer-Targeted and Controlled Drug Delivery. *Adv. Funct. Mater.* **2012**, *22*, 5144−5156.
(17) Angelos, S.; Khashab, N. M.; Yang, Y. W.; Trabolsi, A.; Khatib, H. A.; Stoddart, J. F.; Zink, J. I. pH Clock-Operated Mechanized Nanoparticles. *J. Am. Chem. Soc.* **2009**, *131*, 12912−12914.
(18) Wang, C.; Li, Z. X.; Cao, D.; Zhao, Y. L.; Gaines, J. W.; Bozdemir, O. A.; Ambrogio, M. W.; Frasconi, M.; Botros, Y. Y.; Zink, J. I.; Stoddart, J. F. Stimulated Release of Size-Selected Cargos in Succession from Mesoporous Silica Nanoparticles. *Angew. Chem., Int. Ed.* **2012**, *51*, 5460−5465.
(19) Guillet-Nicolas, R.; Popat, A.; Bridot, J.; Monteith, G.; Qiao, S. Z.; Kleitz, F. pH-Responsive Nutraceutical-Mesoporous Silica Nanoconjugates with Enhanced Colloidal Stability. *Angew. Chem., Int. Ed.* **2013**, *52*, 2318−2322.
(20) Rim, H. P.; Min, K. H.; Lee, H. J.; Jeong, S. Y.; Lee, S. C. pH-Tunable Calcium Phosphate Covered Mesoporous Silica Nanocontainers for Intracellular Controlled Release of Guest Drugs. *Angew. Chem., Int. Ed.* **2011**, *50*, 8853−8857.
(21) Muhammad, F.; Guo, M.; Qi, W.; Sun, F.; Wang, A.; Guo, Y.; Zhu, G. pH-Triggered Controlled Drug Release from Mesoporous Silica Nanoparticles via Intracelluar Dissolution of ZnO Nanolids. *J. Am. Chem. Soc.* **2011**, *133*, 8778−8781.
(22) Liu, R.; Zhang, Y.; Zhao, X.; Agarwal, A.; Mueller, L. J.; Feng, P. Y. pH-Responsive Nanogated Ensemble Based on Gold-Capped Mesoporous Silica through an Acid-Labile Acetal Linker. *J. Am. Chem. Soc.* **2010**, *132*, 1500−1501.
(23) Lee, C. H.; Cheng, S. H.; Huang, I. P.; Souris, J. S.; Yang, C. S.; Mou, C. Y.; Lo, L. W. Intracellular pH-responsive Mesoporous Silica Nanoparticles for the Controlled Release of Anticancer Chemotherapeutics. *Angew. Chem., Int. Ed.* **2010**, *49*, 8214−8219.
(24) Li, L.; Tang, F.; Liu, H.; Liu, T.; Hao, N.; Chen, D.; Teng, X.; He, J. In Vivo Delivery of Silica Nanorattle Encapsulated Docetaxel for Liver Cancer Therapy with Low Toxicity and High Efficacy. *ACS Nano* **2010**, *4*, 6874−6882.
(25) Feng, W.; Zhou, X. J.; He, C. L.; Qiu, K. X.; Nie, W.; Chen, L.; Wang, H. S.; Mo, X. M.; Zhang, Y. Z. Polyelectrolyte Multilayer Functionalized Mesoporous Silica Nanoparticles for pH-Responsive Drug Delivery: Layer Thickness-Dependent Release Profiles and Biocompatibility. *J. Mater. Chem. B* **2013**, *1*, 5886−5898.
(26) Zhu, Y.; Shi, J.; Shen, W.; Dong, X.; Feng, J.; Ruan, M.; Li, Y. Stimuli-Responsive Controlled Drug Release from a Hollow Mesoporous Silica Sphere/Polyelectrolyte Multilayer Core-Shell Structure. *Angew. Chem., Int. Ed.* **2005**, *44*, 5083−5087.
(27) Sun, J.-T.; Hong, C.-Y.; Pan, C.-Y. Fabrication of PDEAEMA-Coated Mesoporous Silica Nanoparticles and pH-Responsive Controlled Release. *J. Phys. Chem. C* **2010**, *114*, 12481−12486.
(28) Zhang, J.; Yuan, Z.-F.; Wang, Y.; Chen, W.-H.; Luo, G.-F.; Cheng, S.-X.; Zhuo, R.-X.; Zhang, X.-Z. Multifunctional Envelope-Type Mesoporous Silica Nanoparticles for Tumor-Triggered Targeting Drug Delivery. *J. Am. Chem. Soc.* **2013**, *135*, 5068−5073.
(29) Sawant, R. M.; Hurley, J. P.; Salmaso, S.; Kale, A.; Tolcheva, E.; Torchilin, V. P. SMART" Drug Delivery Systems: Double-Targeted pH-Responsive Pharmaceutical Nanocarriers. *Bioconjugate Chem.* **2006**, *17*, 943−949.
(30) He, D.; He, X.; Wang, K.; Zou, Z.; Yang, X.; Li, X. Remote-Controlled Drug Release from Graphene Oxide-Capped Mesoporous Silica to Cancer Cells by Photoinduced pH-Jump Activation. *Langmuir* **2014**, *30*, 7182−7189.
(31) Schlossbauer, A.; Dohmen, C.; Schaffert, D.; Wagner, E.; Bein, T. pH-Responsive Release of Acetal-Linked Melittin from SBA-15 Mesoporous Silica. *Angew. Chem., Int. Ed.* **2011**, *50*, 6828−6830.
(32) Yamanaka, H.; Yoshizako, K.; Akiyama, Y.; Sota, H.; Hasegawa, Y.; Shinohara, Y. Affinity Chromatography with Collapsibly Tethered Ligands. *Anal. Chem.* **2003**, *75*, 1658−1663.
(33) Chen, M.; He, X.; Wang, K.; He, D.; Yang, S.; Qiu, P.; Chen, S. A pH-Responsive Polymer/Mesoporous Silica Nano-Container Linked through an Acid Cleavable Linker for Intracellular Controlled Release and Tumor Therapy in Vivo. *J. Mater. Chem. B* **2014**, *2*, 428−436.
(34) Singh, N.; Karambelkar, A.; Gu, L.; Lin, K.; Miller, J. S.; Chen, C. S.; Sailor, M. J.; Bhatia, S. N. Bioresponsive Mesoporous Silica Nanoparticles for Triggered Drug Release. *J. Am. Chem. Soc.* **2011**, *133*, 19582−19585.
(35) Sudimack, J.; Lee, R. J. Targeted Drug Delivery via the Folate Receptor. *Adv. Drug Delivery Rev.* **2000**, *41*, 147−162.
(36) Shi, H.; Cui, W.; He, X.; Guo, Q.; Wang, K.; Ye, X.; Tang, J. Whole Cell-SELEX Aptamers for Highly Specific Fluorescence Molecular Imaging of Carcinomas. *PLoS One* **2013**, *8*, e70476.
(37) Yang, M.; Zhang, X.; Liu, H.; Kang, H.; Zhu, Z.; Yang, W.; Tan, W. Stable DNA Nanomachine Based on Duplex-Triplex Transition for Ratiometric Imaging Instantaneous pH Changes in Living Cells. *Anal. Chem.* **2015**, *87*, 5854−5859.
(38) Ke, C. J.; Su, T. Y.; Chen, H. L.; Liu, H. L.; Chiang, W. L.; Chu, P. C.; Xia, Y. N.; Sung, H. W. Smart Multifunctional Hollow Microspheres for the Quick Release of Drugs in Intracellular Lysosomal Compartments. *Angew. Chem., Int. Ed.* **2011**, *50*, 8086−8089.
(39) Zhou, K. J.; Liu, H. M.; Zhang, S. R.; Huang, X. N.; Wang, Y. G.; Huang, G.; Sumer, B. D.; Gao, J. M. Multicolored pH-Tunable and Activatable Fluorescence Nanoplatform Responsive to Physiologic pH Stimuli. *J. Am. Chem. Soc.* **2012**, *134*, 7803−7811.

DOI: 10.1021/acsami.5b04684
ACS Appl. Mater. Interfaces 2015, 7, 17399−17407

(40) Han, S. Y.; Liu, Y. X.; Nie, X.; Xu, Q.; Jiao, F.; Li, W.; Zhao, Y. L.; Wu, Y.; Chen, C. Y. Efficient Delivery of Antitumor Drug to the Nuclei of Tumor Cells by Amphiphilic Biodegradable Poly(L-Aspartic Acid-co-Lactic Acid)/DPPE Co-Polymer Nanoparticles. *Small* **2012**, *8*, 1596−1606.

DOI: 10.1021/acsami.5b04684
ACS Appl. Mater. Interfaces 2015, 7, 17399−17407